




Deep Transfer Learning with Optimal Deep Belief Network Based Medical Image Classification Model

Paul Thomas Immaculate Rexi Jenifer^{*}, Panchabikesan Nalayini¹, Grace Mary Sebastin¹

School of Computing, SASTRA Deemed to be University, Thanjavur 613401, India

Corresponding Author Email: rexijenifer@cse.sastra.edu

Copyright: ©2024 The authors. This article is published by IIETA and is licensed under the CC BY 4.0 license (<http://creativecommons.org/licenses/by/4.0/>).

<https://doi.org/10.18280/ts.410539>

ABSTRACT

Received: 4 October 2023
Revised: 7 March 2024
Accepted: 15 April 2024
Available online: 31 October 2024

Keywords:

medical image classification, healthcare, deep learning, medical imaging, decision making, parameter optimization

Medical imaging roles an important play in distinct medical applications like medical processes utilized for early recognition, analysis, observing, and treatment evaluation of several clinical conditions. The fundamentals of the rules and executions of artificial neural networks (ANN) and deep learning (DL) are vital to understanding medicinal image analysis from computer vision. A medical image classifier is an essential approach for Computer-Aided Diagnosis (CAD) system. The recent DL approaches offer an effective manner for constructing an end-to-end method which is to calculate last classifier labels with raw pixels of medicinal images. This research gives rise to the MNODBN-MIC model, which stands for MobileNet with optimal deep belief network based medical image classification. There will be multiple class labels applied to the medical images in accordance with the MNODBN-MIC model. The MNODBN-MIC model is able to achieve this objective mainly through the usage of the GF based noise removal methodology. In addition, the MNODBN-MIC model finds the impacted areas by determining a graph-cut based segmentation tool. And feature vectors are also generated using the MobileNet model. Combining the DBN model with elephant herd optimisation (EHO) is the last stage in classifying the data. The EHO algorithm is tasked with adjusting the DBN parameters during this procedure. Using a benchmark dataset, we conduct experimental validation of the MNODBN-MIC model, and the findings show that it outperforms other methods that have been used recently.

1. INTRODUCTION

In recent times, the field of automatic medical image analysis has witnessed a speedy enhancement [1]. The structures illustrated robust estimation abilities and reached similar executions as clinicians [2]. The consolidation of in-depth learning related to automatic medical image interpretations in the clinical routine is presently a famous research topic. The subdomain medical image classification (MIC) focuses to mark a whole image to predefined classes [3, 4]. Recent research has shown that the most efficient and correct MIC pipelines are also greatly dependent on ensemble learning strategy [5]. In the machine learning (ML) domain, the main focus is finding out appropriate hypothesis which increases estimation exactness. Though, identifying the optimum hypothesis is considered very hard that is why the method was developed to merge numerous hypotheses into a prime forecaster nearer to an optimum hypothesis [6, 7]. The combination of ensemble learning strategies in a deep learning related pipeline is known as deep ensemble learning.

New advancements in Deep Neural Networks (DNNs) coupled with a flood of medical images have recently made fast and accurate disease diagnosis possible. To be more precise, it aids neuro-oncologists in making better patient diagnoses and treatment recommendations [8]. The challenges of earlier diagnosing of disorders have risen the significance

of new deep learning methods in medical sciences [9]. One of the major advantages of CNN in comparison to conventional network systems is that it detects important structures automatically and the network structures provide CNN the capacity for learning difficult characteristics from pictures [10]. The new approaches are also enhancing the effectiveness of CNNs and their accurateness.

Masquelin et al. [11] compared discrete wavelet transforms (DWT) with convolutional layer in CNN for evaluating the capability to categorize suspicious lung nodules as benign or malignant. Lai et al. [12] presented a DL method that incorporates Coding Network to Multilayer Perceptron (CNMP) that integrates higher-level features that are extracted from a Deep Convolutional Neural Network (DCNN) and conventional features. Hirano et al. [13] focused on three representation DNN-based medicinal image classification tasks (that is., pneumonia classification, skin cancer, and referable diabetic retinopathy) as well as investigated the susceptibility to the seven structures of UAP. Then, illustrate that DNN is susceptible to non-targeted UAP that causes failure which leads to input allocating an improper class. Huang et al. [14] presented a lightweight hybrid neural network that comprises of adapted PCANet cascaded with DenseNet. The adapted PCANet has two phases where the network generates the efficient feature maps at all the stages via convoluting input with learned kernels. Kowsari et al. [15]

implemented a hierarchical classifier with Hierarchical Medical Image classification (HMIC) method. HMIC employs stack of DL methods for providing understanding at all the levels of the medical image hierarchy.

1.1 Motivation

Medical images are vital for verifying the accuracy of data regarding the human body's anatomy. Diagnostic imaging with digital imaging tools including computed tomography (CT), magnetic resonance imaging (MRI), and positron emission tomography/computed tomography (PET/CT) is becoming important in the medical industry. The development of these technologies is the reason behind this. Considering medical imaging, classifying automatically and retrieval introduces a new radiograph into the archives that exist without interaction, and mostly the images that are retrieved provides a new perspective in making specific diagnoses based on image input. As the pathologic appearance of the images of a person is compared with the image database, clinician is able to make fast and accurate decision, thus reducing cost involved in medical care.

1.2 Scope of the research study

Medical image classification is becoming an integral part of the process of creating computer-aided diagnostic (CAD) models. Conventional CAD models rely largely on the complementing forms, colours, and textures seen in medical imaging, which are problem-oriented. Recent advances in deep learning (DL) have paved the way for a viable method of

creating specialised models for categorization problems. Still, the highest possible resolution of medical images, along with the relatively small datasets, is causing deep learning models to overspend on processing. The proposed study mainly focuses on medical image categorization and offers three different methods to circumvent the limitations mentioned before.

The presented MNODBN-MIC employs Gaussian filtering (GF) based noise removal approach. Also, the MNODBN-MIC model derives a graph cut based segmentation technique to identify the affected regions. Moreover, MobileNet model is exploited to produce feature vectors. Finally, elephant herd optimization (EHO) with DBN model is utilized for data classification in which the EHO algorithm fine tunes the DBN parameters.

2. THE PROPOSED MODEL

In order to sort the medical images into their correct folders, a new MNODBN-MIC model was built specifically for this study. To improve the general quality of medical images, the MNODBN-MIC model primarily used a GF-based noise removal method. Also, to find out what areas are impacted right now, the MNODBN-MIC model provides a segmentation approach using graph cuts. Furthermore, feature vectors are generated using the MobileNet model. In the end, the data is classified using the EHO with DBN model. Figure 1 is a schematic of the MNODBN-MIC method's general procedure.

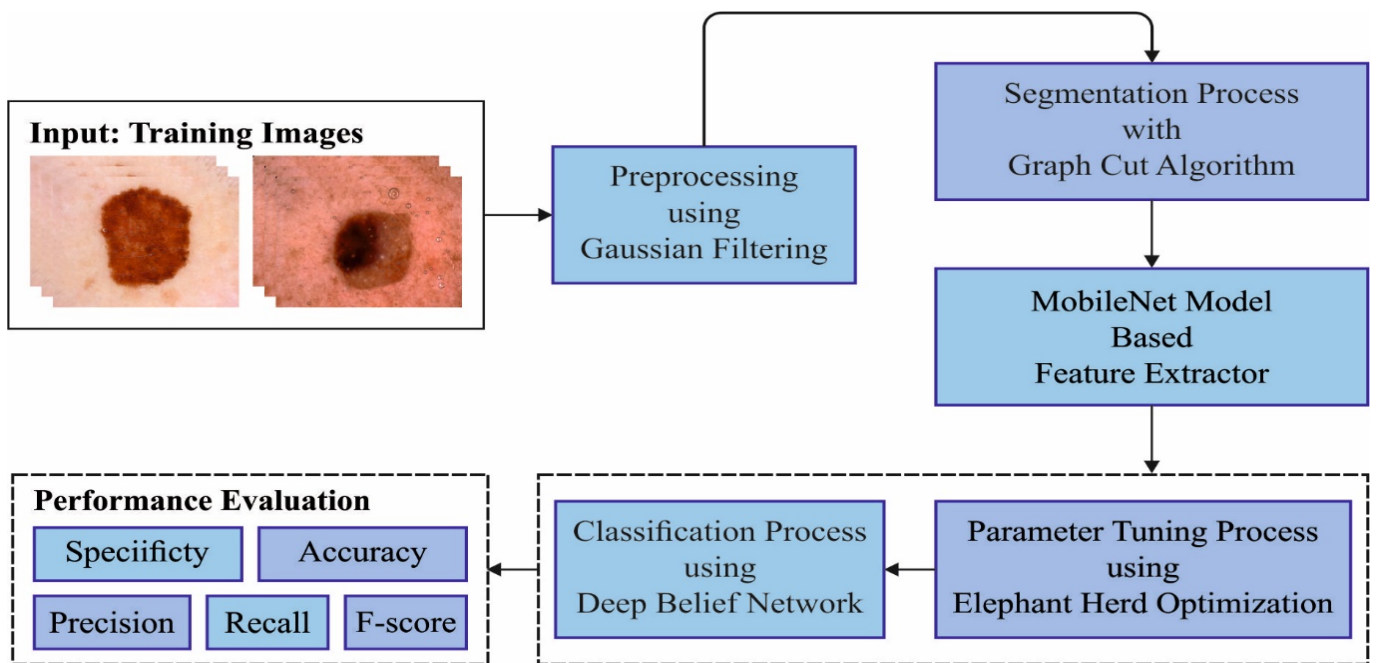


Figure 1. Overall flow of MNODBN-MIC

2.1 Image pre-processing

At its inception, the MNODBN-MIC model relied heavily on GF-based noise removal to improve the medical image quality. The most prevalent uses of a two-dimensional growth function are in the fields of noise reduction and smoothing. The efficiency with which this is executed is inspiring research, because it takes a large amount of processing resources. The

convolutional operator can be utilised to achieve the suggestion of Gaussian smoothness [16], and it is the convolutional operator that describes the Gaussian operator. Here we see the one-dimensional version of the Gaussian operator:

$$G_{1D}(x) = \frac{1}{\sqrt{2\pi}\sigma} e^{-\frac{x^2}{2\sigma^2}} \tag{1}$$

It was essential to localise in both the spatial and frequency domains to obtain the best picture smoothing filter. We were able to achieve this by honouring the uncertainty relationship through:

$$\Delta x \Delta \omega \geq \frac{1}{2} \tag{2}$$

This two-dimensional operator's Gaussian operator is seen in the following equation:

$$G_{2D}(x, y) = \frac{1}{2\pi\sigma^2} e^{-\left(\frac{x^2+y^2}{2\sigma^2}\right)} \tag{3}$$

Here, σ (Sigma) designates the SD of Gaussian function. As soon as it has maximal value, the image smoothing is high. (x, y) signifies the Cartesian coordinate of the images which illustrates the dimension of window.

2.2 Image segmentation

Once the medical images are segmented, the MNODBN-MIC model derives a graph cut based segmentation technique to identify the affected regions. The graph cuts method was usually utilized in medicinal image segmentation because of its benefit in globally optimum solution calculation [17]. As the graph was being sliced:

$$E(f) = (1 - \lambda) \sum_{u \in P} R(f_u) + \lambda \sum_{u \in P, v \in N_u} B(f_u, f_v) \tag{4}$$

The four-neighborhood of pixel u is denoted as N_u , the pixel set of images f is represented by P , the region term $R(f_u)$ punishes separate pixels that are assigned to the object and the background, and the boundary term $B(f_u, f_v)$ punishes a discontinuity between u and v .

$$R(f_u) = \begin{cases} 1 - H(l_u), & \text{if } f_u = \text{tumor} \\ H(l_u), & \text{if } f_u = \text{non-tumor} \end{cases} \tag{5}$$

$$B(f_u, f_v) = \begin{cases} \exp\left(-\frac{(l_u - l_v)^2}{2\eta^2}\right) \cdot \frac{1}{d(u, v)}, & \text{if } f_u \neq f_v \\ 0, & \text{if } f_u = f_v \end{cases} \tag{6}$$

$$\eta = \sqrt{\frac{1}{T_u} \sum_{u \in P, v \in N_u} |l_u - l_v|^2} \tag{7}$$

where, as T_u stands for the pixel number of fixed P .

2.3 Feature extraction

Next to image segmentation, the MobileNet model is exploited to produce feature vectors. Related to other approaches like Inception, it can be established that the MobileNets utilize minimal regularized and dependent upon depthwise separable convolutional but Inception V3 for sample utilized typical convolutional, this outcome as to minimal amount of parameters from MobileNet, but, this outcomes in small reduce from the efficiency so well, thus it can be essential to place a minimum or no weighted decay on depthwise filter as there are several parameters [18].

Specifically, for training the huge methods, it can utilize minimal data-organizing approaches such as executing geometric transformation, as lesser methods are minimal trouble. The size of inputs to the network is also smaller, the output of NN is 3 class labels of 1 crop. The infrastructure of MobileNets was training as well as testing utilizing Python language with Tensorflow CPU library. It can be utilized with other approaches named MobileNetV2 which is a CNN infrastructure that is dependent upon an inverted residual framework, it can be an enhanced version of MobileNet, the fundamental of network remained similar that is a detachable convolutional. Figure 2 showcases the stacked in MobileNet.

Stage	Operator	Resolution	#Channels	#Layers
1	Conv3x3	224 x 224	32	1
2	MBCConv1, k3x3	112 x 112	16	1
3	MBCConv6, k3x3	112 x 112	24	2
4	MBCConv6, k5x5	56 x 56	40	2
5	MBCConv6, k3x3	28 x 28	80	3
6	MBCConv6, k5x5	14 x 14	112	3
7	MBCConv6, k5x5	14 x 14	192	4
8	MBCConv6, k3x3	7 x 7	320	1
9	Conv1x1 and Pooling and FC	7 x 7	1280	1

Figure 2. Stacked in MobileNet

2.4 Image classification

Generally, DBN is composed of restricted Boltzmann machine (RBM) in which all the layers are made up of hidden layer h and visible layer v . The vector w is applied for improving layer connectivity amongst the RBM, and unit existing in the equivalent layer is independent [19]. Energy efficiency can be defined and steady state fo the network corresponding to less power utilization. Thus, it is given in the following:

$$E(v, h) = -\sum_{i=1}^m a_i v_i - \sum_{j=1}^n b_j h_j - \sum_{j=1}^n \sum_{i=1}^m v_i h_j w_{ij} \tag{8}$$

Now a and b indicate the bias vector of visible and hidden layers. Next, the unit of visible and hidden layers are represented as m and n . The conditional and joint distribution for all the layers is defined by following equation:

$$P(v, h) = \frac{e^{-E(v, h)}}{\sum_{v, h} e^{-E(v, h)}} \tag{9}$$

$$P(v | h) = \frac{P(v, h)}{P(h)} = \frac{e^{-E(v, h)}}{\sum_v e^{-E(v, h)}} \tag{10}$$

$$P(h | v) = \frac{P(v, h)}{P(v)} = \frac{e^{-E(v, h)}}{\sum_h e^{-E(v, h)}} \tag{11}$$

Once the unit is not interconnected with each other, the conditional probability of unit is evaluated by following equation:

$$P(h_j = 1|v) = \frac{P(h_j = 1, v)}{P(h_j = 1, v) + P(h_j = 0, v)} \quad (12)$$

$$= \sigma \left(\sum_{i=1}^m a_i + w_{ij}v_i \right),$$

$$P(v_i = 1|h) = \frac{P(v_i = 1, h)}{P(v_i = 1, h) + P(v_i = 0, h)} \quad (13)$$

$$= \sigma \left(\sum_{j=1}^n b_j + w_{ij}h_j \right),$$

$$\sigma(x) = \frac{1}{1 + e^{-x}}. \quad (14)$$

The training procedure of RBM depends on contrast divergence technique as given in the following:

Initialization of parameters. The RBM has hidden layer h and visible layer v applied and developed together with w, a, b whereas learning rate e has minimized arbitrariness. The epochs and batches of RBM are fixed according to the test knowledge. After that, training sample has appeared in the visible layer v .

Update parameters. The conditional probability of hidden layer $h1$ is evaluated by the abovementioned formula. Then, Gibbs sampling method is applied to regenerate $h1$ and v . Based on the regeneration error amongst reconstructed v and actual v , the Stochastic Gradient Descent (SDG) method is employed for variable upgrading w, a, b .

2.5 Hyperparameter optimization

In this work, the EHO algorithm is utilized to fine tune the DBN parameters [20]. The procedure of EHO has been described in the following [20]:

- 1) Elephant belongs to different clans and they live together led by an appropriate elephant. Each clan contains a large number of elephants. In this phase, it is assumed that each clan includes a similar, unchanged number of elephants.
- 2) The place of the elephant in a clan effectively depends on the connectivity for the appropriate elephant.
- 3) The mature male elephant (ME) left the family set and live independently. It is assumed that in each generation, a suitable number of MEs leaves the clan. Therefore, EHO method undergoes the update procedure utilizing a splitting function.
- 4) Generally, the matriarch in each clan is the oldest female elephant (FE). In the operation, resolving, and modeling of the augmented problems, the appropriate elephant is considered by the matriarch separate in the clans.

When the study focuses on improving the EHO update process, it provides further data regarding the EHO update operators.

Assume that an elephant clan is represented by cu . The

succeeding location of elephants v in the clan are upgraded as follows:

$$p_{new,cu,v} = p_{cu,v} + \alpha \times (p_{best,cu} - p_{cu,v}) \times r \quad (15)$$

Here, $p_{new,cu,v}$ indicates the upgraded location, $p_{cu,v}$ denotes the preceding location of elephant v in clan cu . $p_{best,cu}$ denotes the matriarch of clan cu and is the appropriate elephant individually presented in the clan. A scale factor $\alpha \in [0,1]$ determines the control of the matriarch of cu on $p_{cu,v}$. $r \in [0,1]$ indicates a different stochastic distribution provides a significant improvement to various populations in the exploration phase. In our work, uniform distribution was employed.

It should be noted that $p_{cu,v} = p_{best,cu}$, implies that the matriarch in the clan couldn't be upgraded. To avoid this condition, it can be upgraded as the matriarch employing the subsequent formula:

$$p_{new,cu,v} = \beta \times p_{center,cu} \quad (16)$$

in which, the control of $p_{center,cu}$ on $p_{new,cu,v}$, is normalized as $\beta \in [0,1]$. The data from all the individuals in the clan cu is employed to create the new individual $p_{new,cu,v}$. The center of clan cu , $p_{center,cu}$, is calculated to the d -th dimensional searching space in D computation, in which, D indicates the whole dimension in the following:

$$p_{center,cu,d} = \frac{1}{n_{cu}} \times \sum_{v=1}^{n_{cu}} p_{cu,v,d} \quad (17)$$

where, as $1 \leq d \leq D$ denotes the d -th dimensional vector, n_{cu} represent the individual count in cu , and $p_{cu,v,d}$ indicates the d th dimension of individual $p_{cu,v}$.

In elephant clan, ME leaves the family set and lives independently on getting puberty. In the process of divider, it can be modelled by separating an operator when resolving the problem. For enhancing the exploration ability of the EHO method; it is considered that the individual elephant with the bad fitness implemented the separation operator to each generation, as follows:

$$p_{worst,cu} = p_{min} + (p_{max} - p_{min} + 1) \times rand \quad (18)$$

in which, p_{max} and p_{min} denotes the upper and lower bounds, of the location of the individual elephant. $p_{worst,cu}$ indicates the worse elephant in clan cu . $rand \in [0,1]$ indicates stochastic distribution and uniform distribution within $[0,1]$ is employed in the work.

The EHO approach achieves better classifier performance through the construction of an FF. According to this definition, a positive integer represents the best possible performance of potential solutions. In this case, we'll use Eq. (19), which gives us the minimum classifier error rate, as FF. A lower mistake rate indicates a better outcome, whereas a higher rate indicates a worse answer.

$$fitness(x_i) = \frac{ClassifierErrorRate(x_i)}{\text{number of misclassified medical images}} \quad (19)$$

$$= \frac{\text{Total number of images}}{* 100}$$

Pseudo Code of Hyperparameter Optimization using Elephant Herding Optimization (EHO)

```

# Initialization
initialize_parameters() # Initialize DBN parameters and
other EHO-related parameters
# Main
for generation in range(num_generations):
    for clan in elephant_clans:
        for elephant in clan:
            # Update location of elephants in the clan
            update_location(elephant, clan)

            # Apply separation operator for exploration
            if should_apply_separation_operator(elephant):
                separation_operator(elephant, clan)
        # Evaluate fitness of each individual in the population
        evaluate_fitness(elephant_clans)
    # Update matriarchs and explore
    update_matriarchs_and_explore(elephant_clans)
    best_solution = find_best_solution(elephant_clans)
    
```

3. EXPERIMENTAL VALIDATION

Using the HIS2828 Dataset and the ISIC 2017 dataset, this section assesses the MNODBN-MIC model's performance validation. See a couple of picture examples in Figure 3.

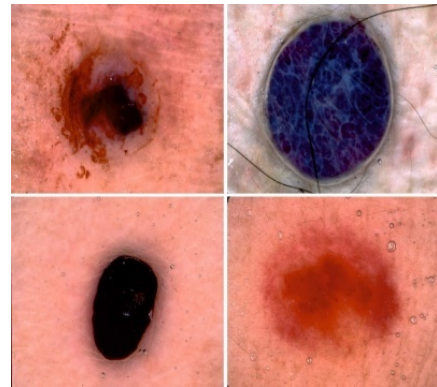


Figure 3. Sample images

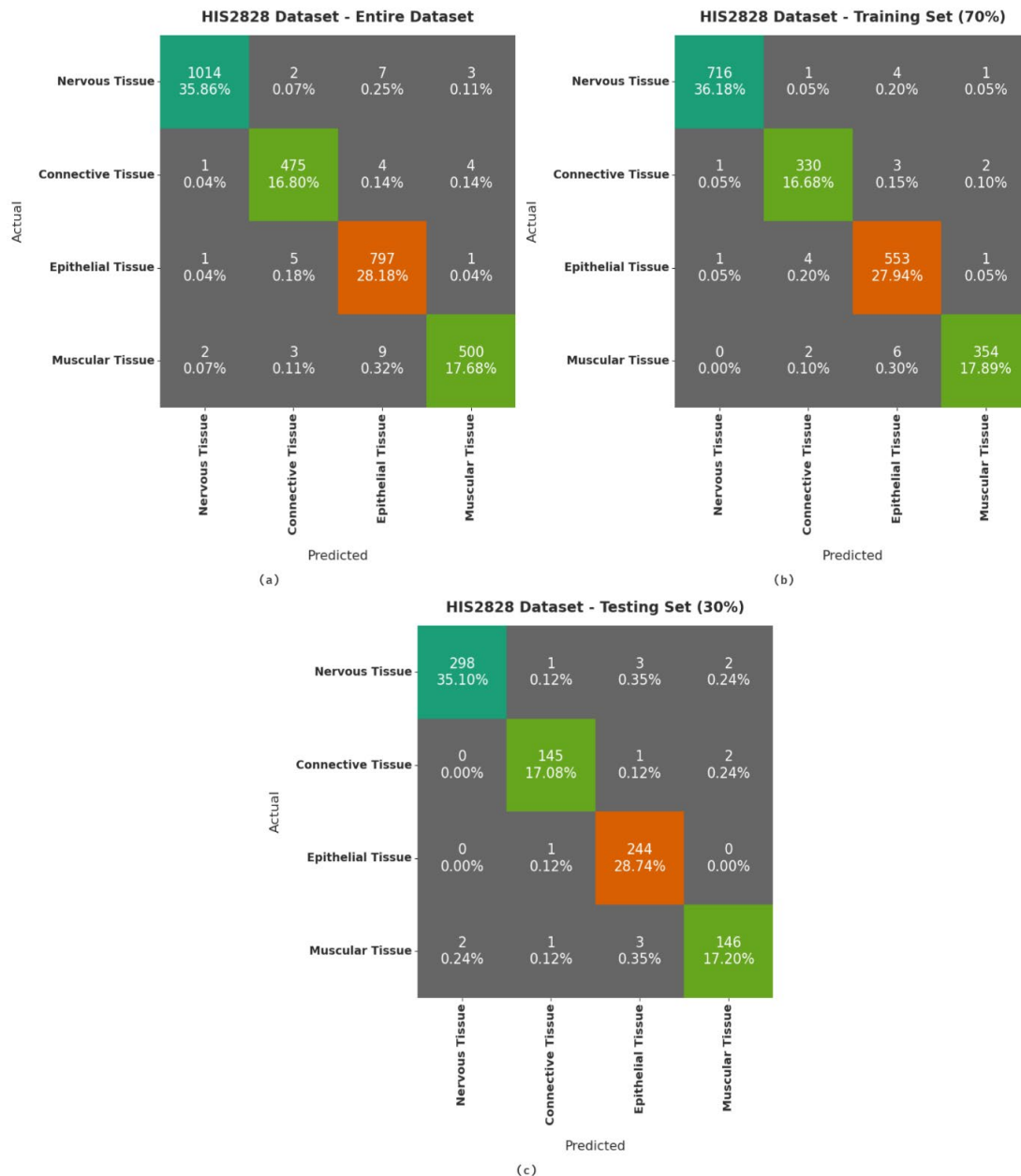


Figure 4. The MNODBN-MIC method's confusion matrix

Table 1. Analysis of the MNODBN-MIC approach's output utilising individual metrics

Class Labels	$accu_y$	$prec_n$	$reca_l$	$spec_y$	F_{score}
Entire Dataset					
Nervous Tissue	99.43	99.61	98.83	99.78	99.22
Connective Tissue	99.33	97.94	98.14	99.57	98.04
Epithelial Tissue	99.05	97.55	99.13	99.01	98.33
Muscular Tissue	99.22	98.43	97.28	99.65	97.85
Average	99.26	98.38	98.34	99.50	98.36
Training (70%)					
Nervous Tissue	99.60	99.72	99.17	99.84	99.44
Connective Tissue	99.34	97.92	98.21	99.57	98.07
Epithelial Tissue	99.04	97.70	98.93	99.08	98.31
Muscular Tissue	99.39	98.88	97.79	99.75	98.33
Average	99.34	98.56	98.52	99.56	98.54
Testing (30%)					
Nervous Tissue	99.06	99.33	98.03	99.63	98.68
Connective Tissue	99.29	97.97	97.97	99.57	97.97
Epithelial Tissue	99.06	97.21	99.59	98.84	98.39
Muscular Tissue	98.82	97.33	96.05	99.43	96.69
Average	99.06	97.96	97.91	99.37	97.93

The confusion matrices generated by the MNODBN-MIC model when applied to the test dataset HIS2828 are shown in Figure 4. Regarding the entire dataset, the MNODBN-MIC model has classified 1014 samples as nerve tissue, 475 as connective tissue, 797 as epithelial tissue, and 500 as muscle tissue, in that order. In addition, 70 percent of the TRS dataset has been classified by the MNODBN-MIC model as nerve tissue (716 samples), connective tissue (330 samples), epithelial tissue (553 samples), and muscle tissue (354 samples). Moreover, out of the thirty percent total surface area dataset, the MNODBN-MIC model has identified 298, 244, and 146 samples that belong to the categories of nerve tissue, connective tissue, epithelial tissue, and muscle tissue, respectively.

Table 1 provides a thorough synopsis of the MNODBN-MIC model's classifier findings on the test HIS2828 dataset. An average result for the entire dataset has been given by the MNODBN-MIC model. $accu_y$, $prec_n$, $reca_l$, $spec_y$, and F_{score} of 99.26%, 98.38%, 98.34%, 99.50%, and 98.36% respectively. In addition, on the 70% of TRS dataset, the MNODBN-MIC model has resulted in average $accu_y$, $prec_n$, $reca_l$, $spec_y$, and F_{score} of 99.34%, 98.56%, 98.52%, 99.56%, and 98.54% correspondingly. Also, on the 30% of TSS dataset, the MNODBN-MIC model has resulted in average $accu_y$, $prec_n$, $reca_l$, $spec_y$, and F_{score} of 99.06%, 97.96%, 97.91%, 99.37%, and 97.93% correspondingly.

The MNODBN-MIC model demonstrated its efficacy on the HIS2828 dataset in terms of both training accuracy (TA) and validation accuracy (VA), as shown in Figure 5. According to the experimental findings, the MNODBN-MIC model has attained the maximum conceivable values of TA and VA. The VA seems to have done better than the TA, to be more specific.

Figure 6 shows the training loss (TL) and validation loss (VL) that the MNODBN-MIC model achieved on the HIS2828 dataset. The experimental results showed that the MNODBN-MIC model got the lowest TL and VL values conceivable. To be more precise, it could seem like the VL is lower than the TL.

The confusion matrices generated by the MNODBN-MIC

model using the test ISIC2017 dataset are shown in Figure 7. Among all samples in the dataset, 371 were classified as Melanoma and 1610 as NS Keratosis according to the MNODBN-MIC model. Also worth noting is that out of the 70% of the TRS dataset that was analysed, the MNODBN-MIC model classified 268 samples as Melanoma and 1120 samples as NS Keratosis. The MNODBN-MIC model has revealed that 103 samples on the 30% TSS dataset are Melanoma and 490 samples are NS Keratosis, adding insult to injury.

Table 2 reports comprehensive results of the MNODBN-MIC model on the test ISIC2017 dataset. On the entire dataset, the MNODBN-MIC model has resulted in average $accu_y$, $prec_n$, $reca_l$, $spec_y$, and F_{score} of 99.05%, 97.84%, 99.11%, 99.11%, and 98.46% correspondingly. In addition, on 70% of TRS dataset, the MNODBN-MIC model has resulted in average $accu_y$, $prec_n$, $reca_l$, $spec_y$, and F_{score} of 99.14%, 98.11%, 99.19%, 99.19%, and 98.64% correspondingly. Also, on the 30% of TSS dataset, the MNODBN-MIC model has resulted in average $accu_y$, $prec_n$, $reca_l$, $spec_y$, and F_{score} of 98.83%, 97.15%, 98.91%, 98.91%, and 98% correspondingly.

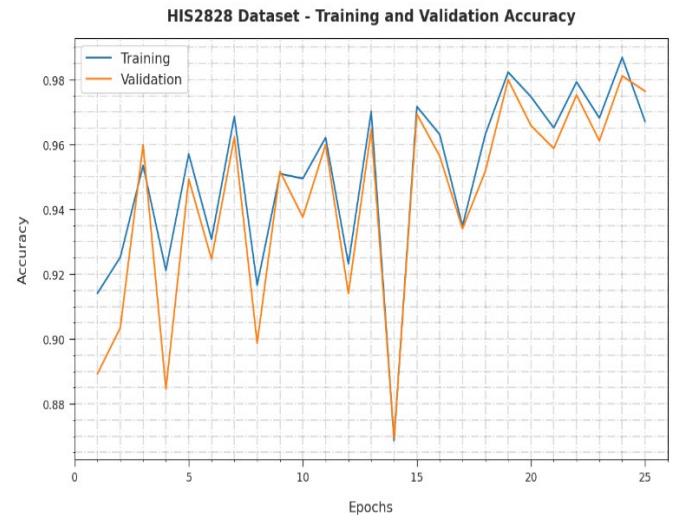


Figure 5. TA and VA analysis of MNODBN-MIC technique

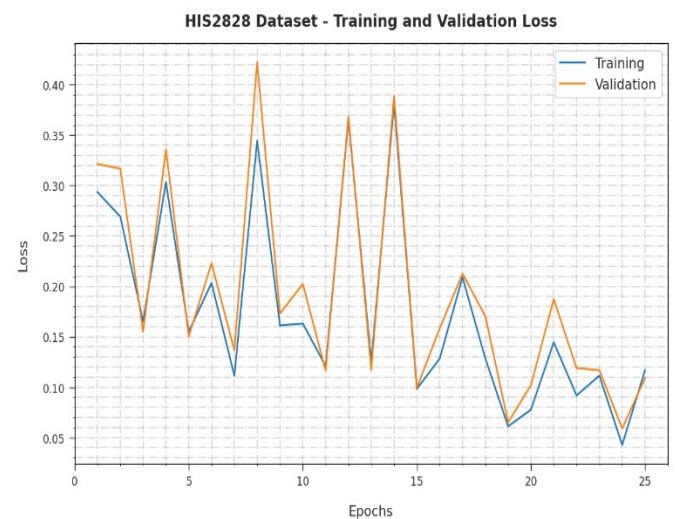


Figure 6. TL and VL analysis of MNODBN-MIC technique

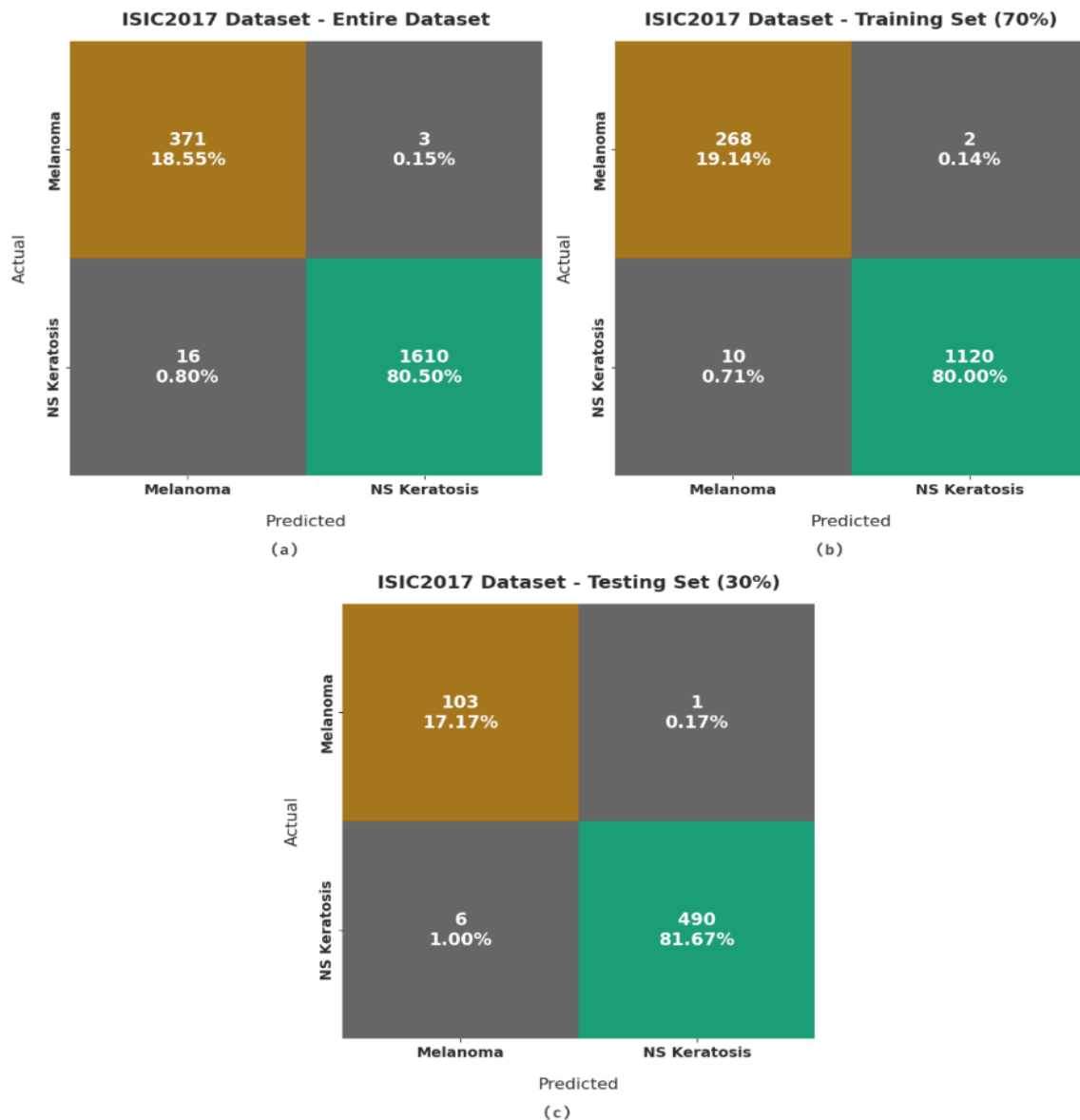


Figure 7. Confusion matrix of MNODBN-MIC technique

Table 2. Result analysis of MNODBN-MIC technique with distinct measures

Class Labels	Accuracy	Precision	Recall	Specificity	F-Score
Entire Dataset					
Melanoma	99.05	95.87	99.20	99.02	97.50
NS Keratosis	99.05	99.81	99.02	99.20	99.41
Average	99.05	97.84	99.11	99.11	98.46
Training (70%)					
Melanoma	99.14	96.40	99.26	99.12	97.81
NS Keratosis	99.14	99.82	99.12	99.26	99.47
Average	99.14	98.11	99.19	99.19	98.64
Testing (30%)					
Melanoma	98.83	94.50	99.04	98.79	96.71
NS Keratosis	98.83	99.80	98.79	99.04	99.29
Average	98.83	97.15	98.91	98.91	98.00

Table 3. Comparative analysis of proposed methods

Proposed Methods	Dataset	Accuracy	Precision	Recall	Specificity
MNODBN-MIC	HIS2828	99.26	98.38	98.34	99.50
	ISIC2017	99.05	97.84	99.11	99.11
DCNN-HSNN	HIS2828	91.09	92.08	97.32	95.97
	ISIC2017	78.82	92.87	94.25	94
IBAS-DTL	HIS2828	97.79	95.64	95.12	98.47
	ISIC2017	98.8	97.4	98.75	98.75

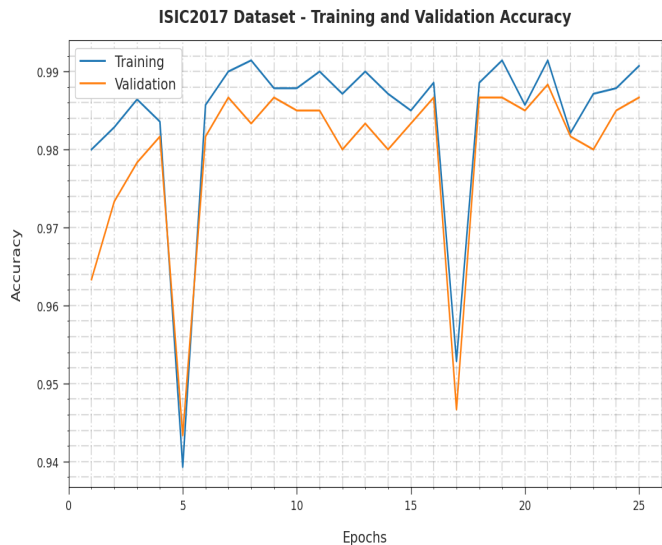


Figure 8. TA and VA analysis of MNODBN-MIC technique on ISIC2017 dataset

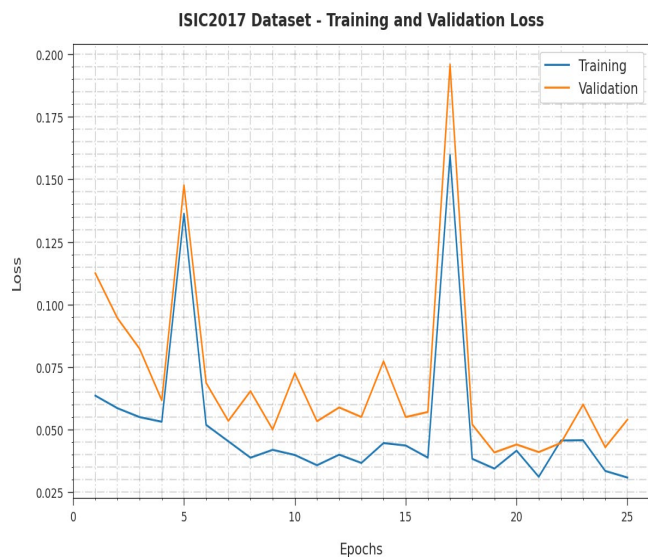


Figure 9. TL and VL analysis of MNODBN-MIC technique on ISIC2017 dataset

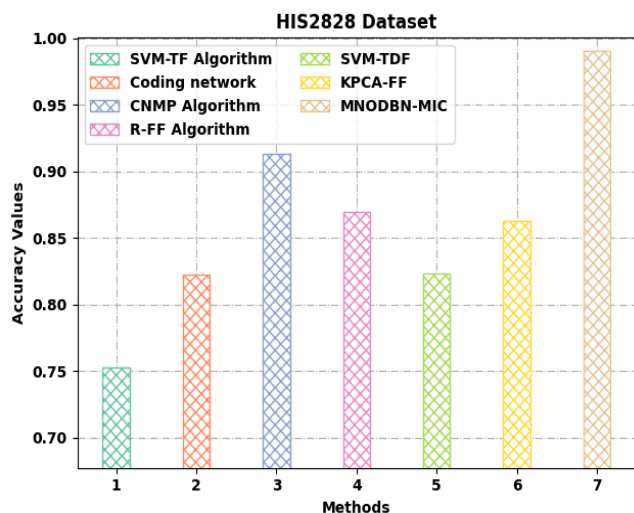


Figure 10. Comparative analysis of MNODBN-MIC technique on HIS2828 dataset

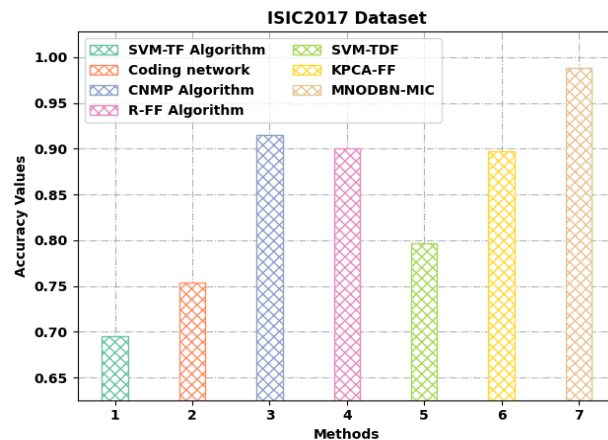


Figure 11. Comparative analysis of MNODBN-MIC technique on ISIC2017 dataset

When applied to the ISIC2017 dataset, the MNODBN-MIC model produced the TA and VA are shown in Figure 8. The experimental results showed that the MNODBN-MIC model got the maximum TA and VA values that could be imagined. In particular, it seems that the VA exceeds the TA sum. Figure 9 displays the TL and VL values generated from the ISIC2017 dataset using the MNODBN-MIC model. The experimental results showed that the MNODBN-MIC model found the lowest TL and VL values that could be achieved. To be more specific, it seems like the VL is below the TL.

On the HIS2828 dataset, Figure 10 displays a thorough evaluation of the MNODBN-MIC model in contrast to newer models. In contrast to the SVM-TF model's 0.7525 accuracy, the coding network and SVM-TDF models achieved marginally better results with 0.8225 and 0.8236, respectively. The figure reported this information. Furthermore, with an accuracy of 0.8691 and 0.8631 respectively. With a maximum accuracy of 0.9906, the MNODBN-MIC model outperforms the other methods. This stands in stark contrast to the 0.9130 accuracy achieved by the CNMP model.

Using more modern models on the ISIC2017 dataset, Figure 11 presents the findings of a complete investigation of the MNODBN-MIC model. According to the figures, the coding network model had a slightly better accuracy of 0.7540 and the SVM-TDF model had a little higher accuracy of 0.7964, but the SVM-TF model had a lower accuracy of 0.6948. Together with this, the R-FF and KPCA-FF models have come near to the actual value, with R-FF at 0.9008 and KPCA-FF at 0.8973. Even though the CNMP model has achieved results that are near the ideal level of accuracy-0.9147-the MNODBN-MIC model outperforms the others with a maximum accuracy of 0.9883.

Thus, the experimental results shown in Table 3 portrayed that the MNODBN-MIC model has resulted in maximum outcomes over the other methods.

4. CONCLUSION

In this study, a new MNODBN-MIC model has been developed to categorize the medical images into distinct class labels. The MNODBN-MIC model primarily employed GF based noise removal approach to optimize medical image quality. In addition, the MNODBN-MIC model derives a graph cut based segmentation technique to identify the

affected regions. Moreover, MobileNet model is exploited to produce feature vectors. Finally, EHO with DBN model is utilized for data classification in which the EHO algorithm fine tunes the DBN parameters. Using a benchmark dataset, we conduct experimental validation of the MNODBN-MIC model, and the findings show that it outperforms other methods that have been used recently. In the future, it will be feasible to improve the performance of the MNODBN-MIC mathematical model using ensemble learning methods.

REFERENCES

- [1] Cai, L., Gao, J., Zhao, D. (2020). A review of the application of deep learning in medical image classification and segmentation. *Annals of Translational Medicine*, 8(11). <https://doi.org/10.21037/atm.2020.02.44>
- [2] Raj, R.J.S., Shobana, S.J., Pustokhina, I.V., Pustokhin, D.A., Gupta, D., Shankar, K.J.I.A. (2020). Optimal feature selection-based medical image classification using deep learning model in internet of medical things. *IEEE Access*, 8: 58006-58017. <https://doi.org/10.1109/ACCESS.2020.2981337>
- [3] Yadav, S.S., Jadhav, S.M. (2019). Deep convolutional neural network based medical image classification for disease diagnosis. *Journal of Big Data*, 6(1): 1-18. <https://doi.org/10.1186/s40537-019-0276-2>
- [4] Zhang, J., Xie, Y., Wu, Q., Xia, Y. (2019). Medical image classification using synergic deep learning. *Medical Image Analysis*, 54: 10-19. <https://doi.org/10.1016/j.media.2019.02.010>
- [5] Azizi, S., Mustafa, B., Ryan, F., Beaver, Z., Freyberg, J., Deaton, J., Loh, A., Karthikesalingam, A., Kornblith, S., Chen, T., Natarajan, V., Norouzi, M. (2021). Big self-supervised models advance medical image classification. In *Proceedings of the IEEE/CVF International Conference on Computer Vision*, Montreal, QC, Canada, pp. 3478-3488. <https://doi.org/10.1109/ICCV48922.2021.00346>
- [6] Jeyaraj, P.R., Samuel Nadar, E.R. (2019). Computer-assisted medical image classification for early diagnosis of oral cancer employing deep learning algorithm. *Journal of Cancer Research and Clinical Oncology*, 145: 829-837. <https://doi.org/10.1007/s00432-018-02834-7>
- [7] Faes, L., Wagner, S.K., Fu, D.J., Liu, X., Korot, E., Ledsam, J.R., Back, T., Chopra, R., Pontikos, N., Kern, C., Moraes, G., Schmid, M.K., Sim, D., Balaskas, K., Bachmann, L.M., Denniston, A.K., Keane, P.A. (2019). Automated deep learning design for medical image classification by health-care professionals with no coding experience: A feasibility study. *The Lancet Digital Health*, 1(5): e232-e242. [https://doi.org/10.1016/s2589-7500\(19\)30108-6](https://doi.org/10.1016/s2589-7500(19)30108-6)
- [8] Wang, W., Liang, D., Chen, Q., Iwamoto, Y., Han, X.H., Zhang, Q., Hu, H., Lin, L., Chen, Y.W. (2020). Medical image classification using deep learning. *Deep learning in healthcare: Paradigms and applications*. Springer, Cham, 33-51. https://doi.org/10.1007/978-3-030-32606-7_3
- [9] Krishnaraj, N., Jayasankar, T., Prakash, N.B., Hemalakshmi, G.R. (2021). Adaptive multimodal image fusion with a deep pyramidal residual learning network. *Journal of Medical Imaging and Health Informatics*, 11(8): 2135-2143. <https://doi.org/10.1166/jmihi.2021.3763>
- [10] Faes, L., Wagner, S.K., Fu, D.J., Liu, X., Korot, E., Ledsam, J.R., Back, T., Chopra, R., Pontikos, N., Kern, C., Moraes, G. (2019). Automated deep learning design for medical image classification by health-care professionals with no coding experience: A feasibility study. *The Lancet Digital Health*, 1(5): e232-e242. [https://doi.org/10.1016/s2589-7500\(19\)30108-6](https://doi.org/10.1016/s2589-7500(19)30108-6)
- [11] Masquelin, A.H., Cheney, N., Kinsey, C.M., Bates, J.H. (2021). Wavelet decomposition facilitates training on small datasets for medical image classification by deep learning. *Histochemistry and Cell Biology*, 155(2): 309-317. <https://doi.org/10.1007/s00418-020-01961-y>
- [12] Lai, Z., Deng, H. (2018). Medical image classification based on deep features extracted by deep model and statistic feature fusion with multilayer perceptron. *Computational Intelligence and Neuroscience*, 2018(1): 2061516. <https://doi.org/10.1155/2018/2061516>
- [13] Hirano, H., Minagi, A., Takemoto, K. (2021). Universal adversarial attacks on deep neural networks for medical image classification. *BMC Medical Imaging*, 21: 1-13. <https://doi.org/10.1186/s12880-020-00530-y>
- [14] Huang, Z., Zhu, X., Ding, M., Zhang, X. (2020). Medical image classification using a light-weighted hybrid neural network based on PCANet and DenseNet. *IEEE Access*, 8: 24697-24712. <https://doi.org/10.1109/ACCESS.2020.2971225>
- [15] Kowsari, K., Sali, R., Ehsan, L., Adorno, W., Ali, A., Moore, S., Amadi, B., Kelly, P., Syed, S., Brown, D. (2020). Hmic: Hierarchical medical image classification, a deep learning approach. *Information*, 11(6): 318. <https://doi.org/10.3390/info11060318>
- [16] Särkkä, S., Sarmavuori, J. (2013). Gaussian filtering and smoothing for continuous-discrete dynamic systems. *Signal Processing*, 93(2): 500-510. <https://doi.org/10.1016/j.sigpro.2012.09.002>
- [17] Feng, J., Wang, X., Liu, W. (2021). Deep graph cut network for weakly-supervised semantic segmentation. *Science China Information Sciences*, 64(3): 1-12. <https://doi.org/10.1007/s11432-020-3065-4>
- [18] Toğaçar, M., Cömert, Z., Ergen, B. (2021). Intelligent skin cancer detection applying autoencoder, MobileNetV2 and spiking neural networks. *Chaos, Solitons & Fractals*, 144: 110714. <https://doi.org/10.1016/j.chaos.2021.110714>
- [19] Sohn, I. (2021). Deep belief network based intrusion detection techniques: A survey. *Expert Systems with Applications*, 167: 114170. <https://doi.org/10.1016/j.eswa.2020.114170>
- [20] Bezdan, T., Milosevic, S., Venkatachalam, K., Zivkovic, M., Bacanin, N., Strumberger, I. (2021). Optimizing convolutional neural network by hybridized elephant herding optimization algorithm for magnetic resonance image classification of glioma brain tumor grade. In *2021 Zooming Innovation in Consumer Technologies Conference (ZINC)*, Novi Sad, Serbia, pp. 171-176. <https://doi.org/10.1109/ZINC52049.2021.9499297>